PRELIMINARY DESIGN OF A WHOLE–ARM MANIPULATION SYSTEM (WAMS)

Kenneth Salisbury[1]
William Townsend[1]
Brian Eberman[1]
David DiPietro[2]

[1]MIT Artificial Intelligence Laboratory, Cambridge, MA 02139
[2]Woods Hole Oceanographic Institute, Woods Hole, MA 02543

ABSTRACT

This paper describes an approach to manipulation that employs all the available manipulation surfaces of the robot to act upon and sense the environment. The kinematic, mechanism, actuation, and control implications of such a design are discussed and initial experimentation with a prototype mechanism are described. A three-degree-of-freedom underwater manipulator employing a number of the resulting design concepts is also described.

1.0 INTRODUCTION

This paper is an overview of our current work on the design and control of experimental arms designed to interact with the environment in a variety of novel ways. We believe that manipulator should be designed from the outset to be able to contact and interact with the environment with any of its surfaces. While current manipulation practice is limited to environmental interaction at the hand of the arm only, there are many instances when it is useful or inevitable to contact the environment with other parts of the arm. Obstacles, that we currently try to avoid, can be used to guide a robot toward its goal. Humans and teleoperated manipulators often use portions of their arm to push and prod items in the environment. Given a fully-loaded hand, humans often clutch an object to their side with their elbow. Earth moving machines often push and pull heavy objects into place. While examples abound of useful whole-arm interactions, there is little analytical or machine experience in such mechanisms (however, see [Mason and Salisbury 85]). Our goal is to understand the underlying design and operational principles of whole-arm manipulators.

Probably of highest importance has been a focus on force control. Since the system is intended to contact objects, sometimes unpredictably, with any part of its mechanism, it is important that forces anywhere along the links be controllable. This in turn implies that joint torque control and sensing be available. Because of the wide range of contact impedances that are possible the force-control system must be particularly robust. For manipulative as well as control reasons we intend to cover most of the manipulator's surface with a high-friction, compliant material. From a workspace point of view we have tried to keep the links' aspect ratios as high as possible (long and slender) in order to maximize the available contact areas. To attain high-aspect-ratio, low-mass, geometrically regular links we strive to keep the actuator volumes inside the link surfaces. The resulting preliminary designs incorporate remotely located actuators which transmit their power to the joints via fast moving cables to efficient reduction mechanisms at the joints. Cables simplify the force-control problem by providing a zero-backlash, smooth transmission medium, and by affording greater flexibility in motor placement. In addition, the cable transmission provides a high degree of backdrivability to each of the joints making it possible to sense link forces from actuator currents. The precise application of torque to the system is achieved by careful feedforward current control of a brushless motor. Our analysis of the sources of motor torque error has led to a practical commutation modification which significantly minimizes torque ripple in the actuators.

To verify some of our initial decisions we have implemented a single-joint test bed embodying a number of the above concepts. The device has been used to test a number of control schemes and to study the accuracy of our dynamic model. This paper then is a brief view of our analysis and implementation of preliminary whole-arm manipulation systems.

2.0 KINEMATIC DESIGN

Designing for whole-arm manipulation poses a whole new set of questions regarding the choice of kinematics appropriate for the pushing, prodding, and novel grasping modes that we envision. While [Salisbury 87] discusses a method of systematically enumerating unique branching kinematic structures capable of unusual manipulation modes, we are devoting our research to developing a series of progressively-more-complex serial-link structures, to illuminate certain design and control issues inherent in this type of manipulation. The first mechanism built was a single-joint device designed to isolate the problems of torque control and transmission in a simple context. The second mechanism is a three-degree-of-freedom manipulator prototype designed to address the issues of reliability and force controllability in an underwater environment.

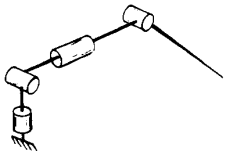

Figure 2.1. 4-degree-of-freedom mechanism kinematics.

Our next device is be a 4-degree-of-freedom mechanism with the kinematics shown in Figure 2.1. This arrangement was chosen because it affords the opportunity to test a number of operational modes utilizing all of the available surfaces. Its capabilities may be viewed in two ways. As a device for simply

positioning or pushing with the end point it has one degree of redundancy and lacks the usual line of singularities along the first rotation axis found in usual three-degree-of-freedom mechanisms [Hollerbach 85]. Alternately, it may be viewed as a device for the positioning of and pushing with a line (the last link). The ensemble of lines reachable with this mechanism consists of all lines passing through the surface of the sphere traced by the endpoint of the first link. Since the last link is not of infinite extent and joint ranges will be less than full, the set of reachable points which the line may contact will be a subset of the above ensemble.

Because of the redundancy available for moving points located on the last link, this last link may be used to contact objects in the environment and exert arbitrarily directed forces upon them, subject to frictional limitations and the need to maintain contact. Similarly, if the last link contacts the environment at an unknown point along its length, the location of the point of contact may be determined by observing the joint torques required to retain contact. Though similar in spirit to the contact sensing described in [Salisbury 84] there are geometric subtleties which must be taken into account. Finally, the arrangement of the two links permits simple inter-link grasping to be demonstrated.

3.0 WAM LINKS AND COVERING

Link geometry is important in whole-arm manipulation. The links must be clean as well as long and slender. By clean we mean that the arm surfaces be able to slide smoothly while in contact with the arm's environment without becoming snagged by wires, linkages, or surface discontinuities present along the arm.

Long and slender links interfere with less of their workspace than fat, short links, and are better at grasping and manipulating as shown in figure 3.1. Figure 3.1 illustrates a serial-link arm trying to grasp a cylindrical object of diameter, D_{cyl}, between consecutive links of length L. In each case the link width, W, and the coefficient of friction, μ, between the object and the cylinder are the same and determine both the the friction-cone angle and the maximum permissible joint angle, θ, which allows a secure grasp. The useful grasping length normalized by the link length, L, is

$$\frac{L'}{L} = 1 - 1/2\frac{W}{L}\frac{1}{\tan\frac{\theta}{2}}, \tag{3.1}$$

and the largest cylinder that the pair of links can grasp is

$$\frac{D_{cyl}}{L} = 2\mu - \frac{W}{L}. \tag{3.2}$$

Therefore, the grasp length, L', and the largest diameter circle that can be grasped are directly dependent on the aspect ratio, L/W.

The four-degree-of-freedom manipulator will have a compliant, friction covering to control contact dynamics and improve grasping quality. The compliance absorbs impact energy and provides the controller time to react to the changing dynamics [An 87]. Additionally, the covering increases the surface friction to allow more secure grasps between the links and objects in the environment. The friction should be Coulombic, because stiction between the covering and the environment compliances causes stick-slip [Rabinowicz 59].

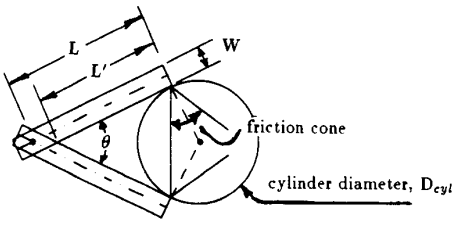

Figure 3.1 Effect of aspect ratio on available contact length.

4.0 ACTUATION

Many early force-control implementations have focused on the use of endpoint force-sensing wrists for closed-loop contact force control. In these implementations, dynamics between the actuator and force sensor have lead to instabilities and bandwidth limitations. An indicated that stable force control could be achieved by removing the endpoint sensor and relying on the accurate control of joint torques [An 86]. Yet accurate torque control via current control is not a trivial matter. [Paul and Shimano 76] used motor currents to infer motor torques. [Wu and Paul 80] developed and implemented a joint torque sensor for a single-joint manipulator. [Luh, Fisher, and Paul 83] implemented closed-loop joint-torque control on the Stanford Manipulator. [Asada 84] noted that hardware limitations are a major obstacle to torque-control implementation. [Dalgetty 84] and [Lim 85] both developed joint-torque sensors for the MIT Direct-Drive Arm having concluded that accurate torque control could not be achieved through current sensing and control. [An 86] utilized current sensing in the MIT Direct-Drive Arm to estimate motor torques but recognized its inaccuracies.

A portion of our research has been aimed at demonstrating that torque sensing is not a requirement for accurate joint-torque control. In our cable-driven arm, an electronically-commutated, Samarium-Cobalt permanent-magnet DC motor, or brushless motor, and a pulse-width-modulated (PWM), controller are utilized for actuation. Manufactured by Moog Inc., the brushless motor and PWM controller offer several advantages over conventional brushed DC-motor technology: reduced mechanical friction, absence of brush arching and wear, reduced rotor inertia, improved heat-dissipation characteristics, and high efficiency.

The output torque of the motor initially included ripples of $\pm$ 10 % of the commanded torque. Some of this ripple could be attributed to transient effects and drift in the controller. This problem was minimized in the latest controller through the use of precision Hall-effect current sensors. Other sources of torque ripple were also identified and addressed. First, the commutation tables were modified to account for scaling factors in the controller. Second, the current loops were carefully calibrated to account for offsets. Finally, the commutation tables were modified to model more-accurately the geometry and

spatial harmonics of the motor. As a result of these efforts, ripple-torque error was reduced below ± 2 % of output torque [Paul 87].

5.0 TRANSMISSION DESIGN

In order to satisfy our geometric requirements for slender, clean links and provide an efficient, smooth, light-weight transmission that is free of backlash, we use cable drives. When pretensioned to at least half the maximum, full-torque tension the cable transmission has linear stiffness and no backlash. Properly-designed, steel-cable drives operating in tension have very high stiffness per unit length for their small mass and can be routed through complex and changing geometries if guided by idler pulleys. The combination of no backlash, low mass, low friction, and geometric flexibility make cable transmissions a good selection for whole-arm manipulators.

5.1 High-Speed Versus Low-Speed Transmissions

One choice which must be made is whether to use a single- or multiple-stage reduction. The torque delivered to the joint is determined by the product of the reduction magnitude, N, and motor torque. If the reduction is done in a single stage, its magnitude is determined by the ratio of the driven-pulley to the drive-pulley diameters. The speed of the cable is determined by the motor-shaft velocity times the drive-pulley radius. Since N is fixed by the torque requirements, the speed of the cable then determines the driven-pulley diameter. If we fix the maximum stress level in the cable, then by doubling the drive- and driven-pulley diameters (and doubling the cable speed), we may use a lighter cable with half the cross-sectional area. Although the cable is lighter, the transmission is twice as stiff. However, the size of the driven pulley will be limited by the geometric need for overall link slenderness (even at the joint).

A more-compact method of implementing a high-speed cable drive is to use a two-stage cabled transmission. The cables are sized so that the cable stress in each stage is the same. If N_{12} is the cable-speed reduction ratio between the first and second stages, then the cross-sectional area of the cable in the second-stage, A_2, is N_{12} times the first-stage area, A_1. If we place N_{12} at a position, x, measured from the motor in a transmission path of length, l; then the effective mechanical torsional stiffness of the transmission, k_{eff}, measured at the link, is

$$k_{eff} = 1/2 \frac{N_{12}^2 R_{driven}^2 A_1 E}{N_{12} l + x(1 - N_{12})}, \qquad (5.1)$$

$$\text{for} \qquad 0 \leq x \leq l \qquad (5.2)$$

where, R_{driven}=the radius of the driven pulley, and E=the effective modulus of elasticity for the cable.

Figure 5.1 shows k_{eff} for several values of N_{12} given a 36-in-long transmission employing a 170-lb-breaking-strength steel cable. k_{eff} increases with N_{12} and for a given N_{12} is maximized by locating the speed reduction at the joint.

Furthermore, if the cable or belt is designed to operate at high speed by using large pulleys in a single-stage transmission or by placing the, N_{12} speed reduction at the joint end rather than the motor end of the transmission in a two-stage transmission, then the distance over which the cables transmit large forces is reduced, thereby lowering internal compressive loads in the link and allowing a lighter link structure.

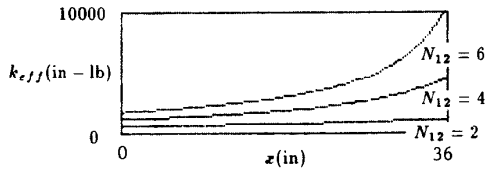

Figure 5.1. Effect of speed-reduction placement on transmission stiffness.

5.2 Sources of Coulomb Friction and Torque Ripple

There are three dominant sources of friction in a cabled transmission — cable-stretch friction, pulley/cable friction, and bearing friction. These three types of friction vary with the preload tension of the cable and the commanded torque output of the joint. [Townsend and Salisbury 87] showed that the Coulomb-like friction caused by cable stretch is proportional to the *square* of the torque load. Second, recent experiments, performed by one of the authors at NASA/JPL, on cable/pulley friction caused by lateral cable compliance show that this friction is stiction-like and *proportional* to cable tension. However, the proportionality does not hold for very-low cable tensions where the resistance goes to some small positive value rather than zero. It has been predicted and shown experimentally [Reynolds 1876] that small-scale slipping between materials, which are compliant in the direction normal to their mutual contact surface, is the source of rolling resistance. Pulley/cable friction may arise from this small-scale slipping which occurs in a limited region near where the cable wraps onto and unwraps from the pulley. Third, it is well known [Marks' Handbook] that ball and roller bearings which support the pulleys have stiction-like friction that is *proportional* to bearing load.

Torque ripple originating in the transmission can also degrade the performance of force control. Beyond the motor-induced torque ripple large torque ripples in cable transmissions can be caused by a small pulley eccentricity, ϵ. These ripples originate from the drive, driven, or idler pulleys and are all proportional to the pretension in the cable circuit. The torque-ripple magnitude, τ_{ripple}, is

$$\tau_{ripple} = 2\epsilon \mathrm{T} \sin\theta \qquad (5.3)$$

where θ is the pulley angular position, and T is the cable pretension. For example, a cable pretension to 50 lb and with a 0.010-in eccentricity would introduce a sinusoidally varying torque of 2 in-lb.

It is important to reduce both the cable tensions and the running preload in order to reduce the resulting friction and increase the dynamic range of force control. Use high speed cables, minimize the manipulator weight which the cables must support, and use active pretension with the use of extra actuators if possible.

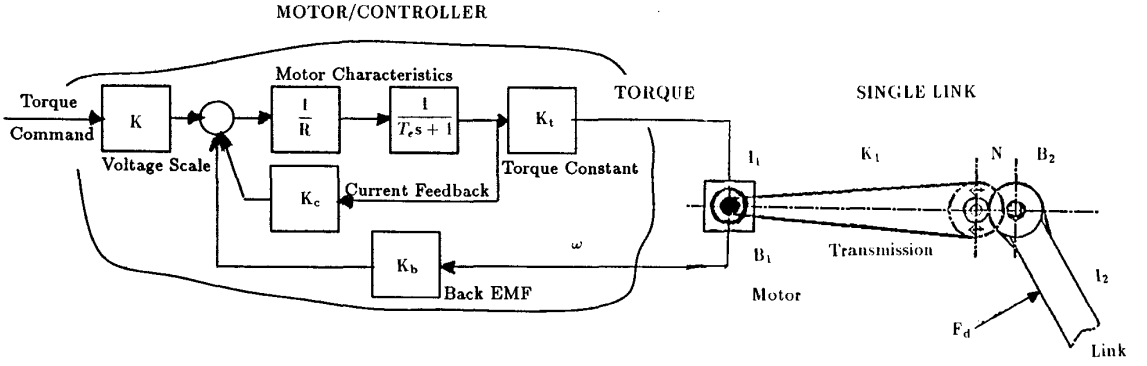

Figure 6.1 Block diagram of open-loop system.

6.0 SINGLE-LINK PROTOTYPE

6.1 Mechanical design of the Single-Link Prototype

A two-stage transmission, shown schematically in figure 6.1, was constructed in preparation for later arm designs. A single-cable circuit spans the 36-in distance between a Moog, DC brushless motor and the joint. The 7x49, stranded construction, 0.044-in-diameter, steel cable has a 170-lb minimum breaking strength and circulates between a 0.75-in drive pulley (at the motor) and a 2.9-in driven pulley. Its stiffness per unit length, EA, has been found to be 9500-lb. A second stage with multiple parallel cables and the same pulley diameters as the first stage is located at the joint and increases the total torque transmission ratio to 14:1. We calculated the *limiting* efficiency attainable with no parasitic friction losses and under the peak motor torque of 60 in-lb to be 0.966 [Townsend and Salisbury 87]. We could have improved the limiting efficiency to 0.983 had we used only a single-stage transmission, but the parasitic losses inherent in present-day ball bearings and in the laterally compliant cables are large enough that this small increase in the limiting efficiency is negligible.

Although the transmission ratio does not match the arm and motor impedances, it is a compromise between the need for good backdrivability, fast acceleration, high torque output, and slender arm geometry. The combined inertia measured at the arm is 65 oz-in-sec^2. The effective arm mass measured at the end tip of the arm is 1.2 lb$_m$. The steady-state and peak torque outputs of the motor are 240 and 960 oz-in respectively. The arm can support its own weight and a 4-lb end-tip load against gravity using steady-state torques. With peak motor torque the arm can apply end-tip forces of 20 lb and rotate half of a revolution from a standstill in 0.25 seconds to an end tip speed of 165 feet-per-second. The stiffness of the end tip of the arm is 12 lb/in when the motor position is locked.

6.2 Dynamic Model of the Single-Link Prototype

A dynamic model of the system was developed to help evaluate the link design and to assist in formulating the control laws for the future 4-degree-of-freedom manipulator. Based on this dynamic model, the structural modes of the system were identified and compared experimental results. The link, transmission and motor can be modeled as an inertia and a pendulum coupled by a single spring with damping to ground at both the pendulum and the inertia. The compensator used for closed-loop control contains a feedforward correction term for the effects of gravity. This leads to a linearization of the equations of motion and results in the form:

$$\dot{x} = Ax + Bu \qquad \text{where} \qquad x = (\theta_1 \dot{\theta}_1 \theta_2 \dot{\theta}_2 i)^T, u = (CF_d)$$

$$A = \begin{pmatrix} 0 & 1 & 0 & 0 & 0 \\ -\frac{K_1}{I_1} & -\frac{B_1}{I_1} & \frac{(K_1 N)}{I_1} & 0 & \frac{K_t}{I_1} \\ 0 & 0 & 0 & 1 & 0 \\ \frac{K_1 N}{I_2} & 0 & \frac{-K_1 N^2}{I_2} & -\frac{B_2}{I_2} & 0 \\ 0 & -\frac{K_b}{RT_e} & 0 & 0 & -\frac{K_c + R}{RT_e} \end{pmatrix}, \quad B = \begin{pmatrix} 0 & 0 \\ 0 & 0 \\ 0 & 0 \\ 0 & \frac{1}{I_2} \\ \frac{K}{RT_e} & 0 \end{pmatrix} \tag{6.1}$$

where the constants and states are shown by figure 6.1.

The response of the system is governed by four transfer functions. Transfer functions can be formed between the motor input torques and each of the two mass positions and between disturbance forces acting on the surface of the link and each of the two mass positions. For a single-input, single-output controller only two of these transfer functions are needed with a colocated sensor. Eppinger and Seering demonstrated that the use of noncolocated sensors in a force-control scheme led to instabilities because of the structural dynamics between the actuator and the sensor [Eppinger and Seering 86]. Based on this result, we have chosen to use only the colocated resolver on the Moog motor for control of the single link. The colocated transfer functions for this control structure are given by:

$$G_1(s) = \frac{\theta_1(s)}{C(s)} = \frac{K K_t (I_2 s^2 + B_2 s + K_1 N^2)}{s(\alpha s^4 + \beta s^3 + \gamma s^2 + \delta s + \epsilon)} \tag{6.2}$$

$$G_2(s) = \frac{\theta_1(s)}{F_d(s)} = \frac{K_1 N (R T_e s + R + K_c)}{s(\alpha s^4 + \beta s^3 + \gamma s^2 + \delta s + \epsilon)} \tag{6.3}$$

where the values of the constants can be determined from equation 6.1.

A plot of the open-loop poles and zeros of the colocated transfer function from the motor torque command to the link output position reveals that the response is governed by a rigid-body pole, a pole on the real axis determined by the damping on the inertias, a pole on the real axis introduced by the motor dynamics, a pair of lightly-damped poles, and a lightly-damped pair of zeros. The natural frequency of the lightly-damped pole pair can be identified as the natural frequency of the two masses

and the transmission spring and is defined as ω_n. Based on the design, ω_n was predicted to be about 73 Hz. Using a Hewlet Packard Structural Analyzer, ω_n was found to be at 67 Hz. The pair of zeros in $G_1(s)$ occur at the natural frequency of the single link vibrating against the transmission with the motor fixed and is defined as ω_1. Analysis of the design predicted that ω_1 would occur at 10 Hz and was experimentally determined to be 8.2 Hz. The system model is shown by the block diagram in Figure 6.1 and the open-loop pole-zero plot shown in Figure 6.2.

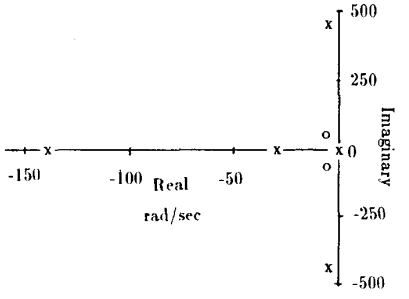

Figure 6.2 Pole-zero plot of open-loop system.

6.3 Force and Stiffness Control of Single Link

A digital controller using a VAX 11/750 running at 50 Hz was built to perform force-control experiments with the single-link. The control system contains compensation for the known non-linearities, a digital differentiator, a digital filter for the velocity signal, and two adjustable gains. In addition, to decrease the noise on the joint potentiometer associated with the 5 KHz PWM power supply, a 6th-order lowpass butterworth analog filter with a cutoff frequency of 25 Hz was incorporated into the system. A block diagram of the entire control system is shown in figure 6.3.

Using this controller, the stiffness and damping linearity and the force-control capabilities of the link were investigated. Well-damped stiffnesses at the output joint axis from 0 in-lb/rad to 2000 in-lb/rad (1.5 lb/in at the link tip) and pure dampers from 0 in-lb/rad/s to 200 in-lb/rad/s (.15 lb/in/sec) were obtained with the system. Of critical importance to WAM is the ability of the link to perform stably in a real environment. Initial experiments have shown the link to be stable while applying forces or colliding with both hard and soft environments for the stiffness and damping ranges previously given.

Based on the force and stiffness control experiments and the dynamic model, we have developed a few design rules. Although for high gains the poles at ω_n will become unstable, placing a stability limit on stiffness, well damped behavior is limited by the location of the zeros of $G_1(s)$ at ω_1. This frequency is controlled by the stiffness of the cables, the mass of the link, and primarily by the transmission ratio. In order to improve the performance of the system the frequency should be maximized by maximizing the transmission stiffness, and by link mass. Greater stability may be attainable for high stiffnesses by shifting the poles to the left with the addition of

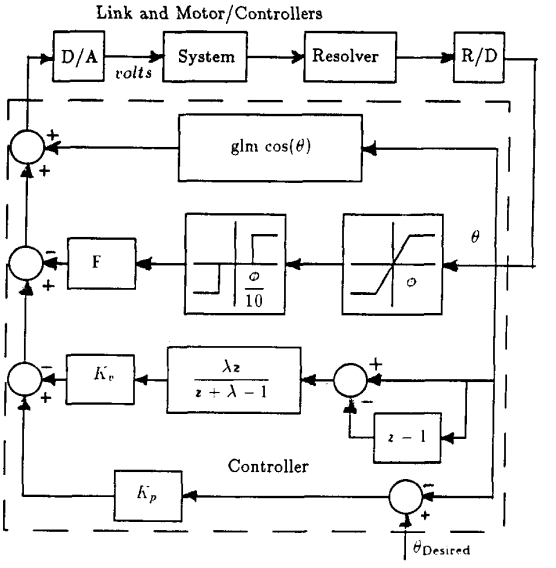

Figure 6.3 Block diagram of system with controller.

passive damping.

The effects of backlash were demonstrated by the keyway in the system. The motor shaft is connected to the drive pulley by a glued-in keyway. Although the connection made between the motor shaft and the drive pulley appeared to be solid, a

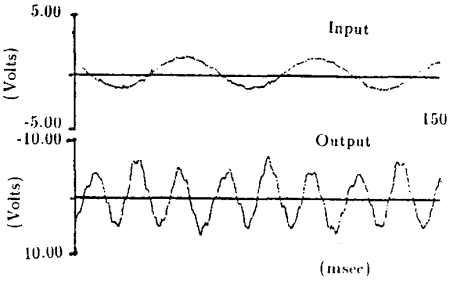

Figure 6.4 Plot of superharmonic response of system.

nonlinear cubic spring effect was observed when the motor was excited with a 20-Hz sine wave. As shown in figure 6.5, when the motor controller was driven with a 20-Hz sine wave the acceleration measured on the drive pulley was at 60 Hz. At input frequencies below 20 Hz the frequency of the output was at the input frequency but the waveshape was no longer a clean sine wave. Above 20 Hz, the response was cleaner and most coherent at ω_n.

7.0 3-DOF UNDERWATER PROTOTYPE

The three-degree-of-freedom manipulator designed at the Deep Submergence Laboratory of the Woods Hole Oceanographic Institution is part of the JASON remote-control underwater-vehicle project. The vehicle/manipulator system, scheduled for completion in 1988, will be used by scientists and the

Navy to explore the ocean floor to depths as great as 6000 m. Tasks which the manipulator will be required to perform will range from engaging two underwater connectors, to lifting loads as great as 20 lb at the full 30-in extension, to retrieving delicate organic samples for investigation. In order to execute a broad array of unstructured tasks effectively, the manipulator needs a zero-backlash, low-friction actuator package which is backdriveable.

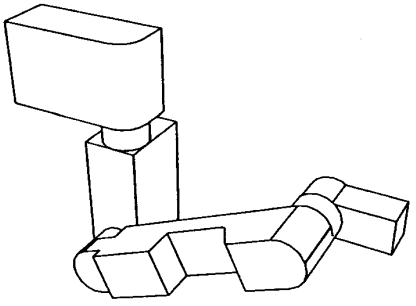

Figure 7.1. 3-degree-of-freedom underwater-manipulator prototype.

The link arrangement shown in figure 7.1 was found most appropriate because it allows for excellent obstacle avoidance and it occupies and sweeps out less volume than comparable parallel-link mechanisms. Link three is offset from link two to allow it to rotate 360 degrees and thus be stowed next to link two when the manipulator is not needed. Three rotary axes were considered sufficient for this initial device to demonstrate a number tasks requiring force control underwater. Furthermore, the vehicle itself can provide an additional six degrees of freedom (of much lower bandwidth, however).

All wires are enclosed in the housings and pass from link to link through the joint torque tubes. Space has been provided internally for video and hydraulic lines, should they be deemed necessary for work tasks. Link two has a fairly complicated geometry primarily because efforts were made to reduce its cross-sectional area, and thus the entrained water when the link moves. The entire manipulator is filled with oil, which serves as a lubricant, a pressure compensation fluid, and a source of buoyancy.

The decision to use the same motor for all three rotational axes was based on financial as well as operational concerns. Having common motors, controllers, and drivers means components can be interchanged easily and a smaller inventory is required—important features when considering the difficulty of operating from the cramped quarters of a research vessel. Seiberco DC brushless "Sensorimotors" were selected because of their very high torque-to-weight ratio, high motor constant, low torque ripple, and built-in velocity and position sensor. Thus the motor has no add-on sensors, making it constructionally simple and small. The controller runs a high-bandwidth torque servo eliminating the need for torque sensors.

The actuation package for each joint consists of a specially-designed, low-speed Sensorimotor driving a cable transmission. Operating speeds of the motor were designed to fall between 0 and 600 rpm. Higher speeds cannot be utilized, because high-speed motion underwater is impractical. A reduction ratio of 30 to 1 was selected for the first and second axes, while the third axis is driven through a 13-to-1 reduction. The reducers of the first two axes are identical three-stage systems consisting of stainless-steel cables wrapped around pulleys. A three-stage system was chosen to provide a fairly-high reduction ratio without making the pulleys, and thus the manipulator housing, too large.

The higher reduction allows the motors to be run at higher, more-efficient average speeds, tends to cause better filtering of torque ripple, provides a higher effective motor constant than comparable direct-drive systems and gives high position resolution without expensive sensors all in a fairly-light actuator package. Calculations indicate that the cable transmission efficiency *limit* is greater than 98.5%, as opposed to roughly 99% for a two-stage system. For the moment, losses due to bearing, seal, and lateral cable compliance prevent us from attaining this theoretical limit. The output stage of the reduction has four 1/16-in-diameter cables in parallel to allow the manipulator to accommodate heavy loads. Successive stages have two sets and then one set of cables, in proportion to the reduced tension they experience.

Cables must be run in parallel if a high-strength, compact system is to be designed. While increasing cable diameter is one way of allowing for higher cable tension, and decreasing the number of parallel cables, it implies that larger-diameter pulleys must be used if the minimum bend radius of the cable is not to be exceeded. To ensure equal loading of all parallel

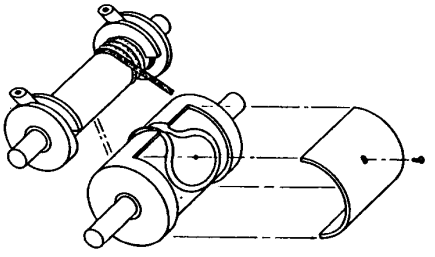

Figure 7.2. Cable-tension balancing scheme.

cables, and thus have a fatigue-resistant design, a method must exist for equalizing the tension in each cable. The scheme used on the output stage of the shoulder reducers allows a single piece of cable to change direction three times and thus act as four cables in parallel. Figure 7.2 shows an example of this idea. Because the grooves on the surface of each pulley have sufficiently large radii, the cable is fatigued no more than it would be if it were running over one of the smallest pulleys. In addition, the large radius allows the cable to slip and therefore equalize its tension during pretensioning.

All cable circuts are pretensioned. This makes the circuits twice as stiff as if they were not pretensioned, and also avoids an;y possibility of backlash. Pretensioning is acomplished at the input stage via a scheme which propagates pretension (proportionally) through all three stages.

In an effort to reduce the overall complexity of the design,

and thus the likelihood of malfunction, the manipulator uses only colocated located actuator sensors which are integral with the motor stator. Since estimation of cable stretch will be used to improve endpoint positioning accuracy under load, seal and bearing-friction induced forces have been minimized by careful component selection. Because the motors were designed to provide excellent torque control, no method has been provided to measure the joint torque directly. The assumption is made, based on manufacturer's specifications, that a linear relationship exists between torque and motor current, and thus tight current control infers accurate torque control.

As discussed earlier, actual output torque may vary as a result of imperfections in the transmission and reduction construction. The motors themselves have less than $\pm$ 2% torque ripple, measured as a percent of maximum torque. While this is fairly low, it causes uncertainty in the torque-control schemes. It is anticipated that appropriate motor-controller modifications, including electronic and the feedforward techniques discussed in section 4 will reduce the problem.

The prototype manipulator described above was developed to demonstrate the feasibility of high-performance cable transmissions and reductions in a wide-dynamic-range manipulator, operating in a very-demanding, unstructured environment. The design represents the result of compromises which were made to ensure functionality in the field, but even with the modifications necessary to take the single-link prototype from the lab to the ocean, the system should represent a significant improvement over existing underwater manipulators.

8.0 CONCLUSIONS

This paper really addresses two central issues in the development of manipulators which are able to take greater advantage of their structure to manipulate and perceive objects in their environment. From a kinematic point of view we have identified a number of constraints which must be observed in order to utilize manipulator surfaces for effectively pushing, grasping, and sensing objects. From a design point of view we have developed an approach to building force-controllable mechanisms which takes advantage of accurate torque generation, efficient transmission design, and a simple mechanical structure.

Central to our research is the building of a series of progressively more complex and capable mechanisms aimed at helping us gain experience in whole-arm manipulation and control. While the potential benefits of being able to utilize more fully manipulator actions are enormous, such utilization will require solutions to many untouched and challenging design, control, and planning problems.

ACKNOWLEDGMENT

The authors would like to gratefully acknowledge the finincal assistance of the Office of Naval Research for support in this research. At the MIT AI Lab the work was performed under ONR contracts N00014-86-K-0685 and N00015-85-K-0124 and at the Woods Hole Oceanographic Institute the work was performed under ONR grant N-00014-87-G-0112 and ONR contract N00014-86-C-0038.

REFERENCES

An, C.H., "Trajectory and Force Control of a Direct Drive Arm," MIT AI Technical Report AI-TR-912, MIT Artificial Intelligence Lab, Cambridge, MA, 1986.

Asada, H., Youcef-Toumi, K., and Lim, S.K., "Joint Torque Measurement of a Direct-Drive Arm," *23d IEEE Conference on Decision and Control*, pp. 1332–1337, Dec., 1984.

Brock, D. L., "Enhancing the Dexterity of a Robot Using Controlled Slip", Report AI-TR-992, MIT AI Laboratory, October, 1987.

Dalgetty, B.L., "Joint Torque Sensor for a Direct-Drive Arm," Master's Thesis, Massachusetts Institute of Technology, 1984.

Eppinger, S.D., Seering W.P., "On Dynamic Models of Robot Force Control", *Proc. IEEE International Conference on Robotics and Automation*, San Francisco, CA, April, 1986.

Hollerbach, J.M., "Optimum Kinematic Design for a Seven Degree of Freedom Manipulator," *Robotics Research: The Second International Symposium*, ed. H. Hanafusa and H. Inoue, MIT Press, Cambridge, MA 1985.

Lim, S.K., "Measurement and Control of Joint Torque for a Direct-Drive Arm," Master's Thesis, Massachusetts Institute of Technology, 1985.

Luh, J.Y.S., Fisher, W.D., and Paul, R.P., "Joint Torque Control by a Direct Feedback for Industrial Robots," *IEEE Transactions on Automatic Control*, AC-28, pp. 153–160, 1983.

Marks' Standard Handbook for Mechanical Engineers, 8th ed., edited by T. Banmeister, McGraw-Hill, NY 1978, pp. 8–140.

Mason, M.T. and Salisbury, J.K., *Robot Hands and the Mechanics of Manipulation*, MIT Press, Cambridge, MA, 1985.

Paul, B.,"A Systems Approach to the Torque Control of a

Permanent Magnet Brushless Motor," Master's Thesis, Massachusetts Institute of Technology, 1987.

Paul, R.P., and Shimano, B.,"Compliance and Control," *Proceedings of the Joint Automatic Control Conference*, pp. 694–699, 1976.

Rabinowicz, E. "A Study of the Stick-Slip Process," published in *Friction and Wear*, Ed. by Robert Davies, Elsevier Pub. Co., New York, 1959.

Reynolds, O., "On Rolling-Friction," *Philosophical Transactions of the Royal Society of London*, Vol. 166-Part I, London, England, 1876.

Salisbury, J.K. "Whole-Arm Manipulation," Proceedings of the 4th International Symposium of Robotics Research, Santa Cruz, CA, August, 1987. Published by the MIT Press, Cambridge MA.

Salisbury, J.K., "Interpretation of Contact Geometries from Force Measurements," *Proc. 1st International Symposium on Robotics Research*, Bretton Woods, NH, MIT Press, Sept., 1984.

Townsend, W.T. and Salisbury, J.K., "The Effect of Coulomb Friction and Stiction of Force Control," *Proc. 1987 IEEE International Conference on Robotics and Automation*, Raleigh, North Carolina, April, 1987a.

Townsend, W.T. and Salisbury, J.K., "The Efficiency Limit of Belt and Cable Drives," submitted for publication in the *ASME Journal of Mechanisms, Transmissions, and Automation in Design*, June, 1987b.

Wu, C.H. and Paul, R.P., "Manipulator Compliance Based on Joint Torque Control," *19th IEEE Conference on Decision Control*, pp. 88–94, Dec., 1980.